NASA

Technical Memorandum 85098

ORBIT DETERMINATION AND PREDICTION STUDY FOR DYNAMIC EXPLORER 2

R. L. Smith, Y. Nakai, and
C. E. Doll

OCTOBER 1983

National Aeronautics and
Space Administration

Goddard Space Flight Center
Greenbelt, Maryland 20771

TM 85098

ORBIT DETERMINATION AND PREDICTION STUDY FOR DYNAMIC EXPLORER 2

R. L. Smith
Computer Sciences Corporation

Y. Nakai
Computer Sciences Corporation

C. E. Doll
Goddard Space Flight Center

October 1983

GODDARD SPACE FLIGHT CENTER
Greenbelt, Maryland

ABSTRACT

Definitive orbit determination accuracy and orbit prediction accuracy for the Dynamic Explorer-2 (DE-2) are studied using the Goddard Trajectory Determination System for the period within six weeks of spacecraft re-entry. Baseline accuracies using standard orbit determination models and methods are established. A promising general technique for improving the orbit determination accuracy of high-drag orbits, estimation of random drag variations at perigee passages, is investigated. This technique improved the fit to the tracking data by a factor of five and improved the solution overlap consistency by a factor of two during a period in which the spacecraft perigee altitude was below 200 kilometers. The results of the DE-2 orbit predictions showed that improvement in short term prediction accuracy reduces to the problem of predicting future drag scale factors; the smoothness of the Solar 10.7-centimeter flux density suggests that this may be feasible.

ACKNOWLEDGMENT

This work was supported by the Orbiting Satellites Project/Science Code 602 of the Sciences Directorate at Goddard Space Flight Center under the direction of J. P. Corrigan. The authors would like to acknowledge the technical contributions made by J. Teles of Goddard Space Flight Center.

CONTENTS

ORBIT DETERMINATION AND PREDICTION STUDY FOR DYNAMIC EXPLORER 2

SECTION 1 – INTRODUCTION

In this study the accuracy of orbit determination and orbit prediction for a low-altitude spacecraft are evaluated for the final weeks of drag decay prior to re-entry. For this project, the Dynamic Explorer-2 (DE-2) was more intensively tracked than was customary for operational, end-of-lifetime orbit determination, and this additional tracking was intended to permit increased orbit accuracy in operational-type solutions through local improvement in the drag force modeling. The results of this study establish baseline navigation performance using the current orbit computation system, for application to future projects and for comparison with future TDRSS performance for low-altitude spacecraft.

Force model errors are the major source of orbit determination error for arc lengths in excess of a few revolutions, when NASA S-band tracking data (range and Doppler) is used. Of course, for end-of-lifetime solutions it is expected that errors in drag force modeling will comprise the major source of orbit determination and orbit prediction errors. During the periods of tracking studied, the DE-2 orbit was at altitudes between 200 and 380 kilometers. In an earlier study (Reference 1) for the High Energy Astronomy Observatory (HEAO-2), in which the spacecraft was at an altitude of 500 kilometers, definitive orbit determination errors of about 50 meters were obtained using readily available gravity and drag models. At the lower DE-2 altitudes considered in this study, the errors are substantially larger, and part of the purpose of this work was to establish these error levels.

In Section 2 of this report, the available DE-2 tracking data and the orbit determination and orbit prediction methods are described. In Section 3, rough estimates of the effects of gravity model and drag model errors are presented. In Section 4, the numerical results of the study are given.

For definitive orbit determination these include the effects of different gravity and atmosphere models, the effects of definitive solution arc length, and the effects of modifying the force model using impulsive perturbations in an attempt to reduce drag errors. For orbit prediction, numerical results showing the effect of the predicted drag force scale factor are given. Finally, Section 5 contains the conclusion, indicating directions for future work suggested by the results.

SECTION 2 – DATA AND METHODS

2.1 DE-2 ORBIT CHARACTERISTICS AND TRACKING DATA

Orbital parameters for DE-2 are summarized in Table 1. The orbit is polar with low eccentricity, and although the eccentricity is low, the variation in the altitude during one revolution is sufficient to cause an order of magnitude difference in the drag force between apogee and perigee. Figure 1 shows the decrease in apogee and perigee altitudes prior to re-entry on February 19, 1983.

NASA Unified S-band range and Doppler tracking data was used to determine the orbits in this study. The amounts of tracking available are shown in Figure 2. Approximately equal numbers of range and Doppler observations were available and used. It was originally desired that about 18 to 20 passes of tracking per day be obtained, which was estimated as the maximum available with the geometrical limitations of ground-based tracking; however, as indicated by Figure 2, the average rate actually obtained was 10 to 12 passes per day. Consequently, only modest improvements in orbit accuracy could be expected in the results of this study.

2.2 ORBIT DETERMINATION AND PREDICTION METHODS

Four periods of time, each approximately three days in length, were selected for study. The relationship of these selected periods to the orbital altitudes and to the tracking data distribution is shown in Figures 1 and 2. Orbit solutions within these periods were calculated using the Goddard Trajectory Determination System (GTDS) (Reference 2), either the operational version or a slightly modified operational version. Definitive orbit solutions were overlapping, by 6 hours for the 18-hour solutions or by 8 hours in the case of a single group of 32-hour solutions. Maximum ephemeris differences within the overlap intervals were used as a gauge of definitive solution accuracy, recognizing that reduced overlap differences are a necessary, but not sufficient condition for improved orbit accuracy.

For the predictive orbit accuracy studies, predictive trajectories started at the epochs of definitive orbit solutions in period 1 and were stopped at the end of period 2. The accuracy of the predicted trajectories was measured by comparison with definitive solutions. In these comparisons, the maximum position differences were calculated for 6-hour periods at repetitive intervals of one day, so that the growth of the predictive error could be observed.

Two Earth gravity models were used and compared in this study: the Goddard Earth Model 9 (GEM9) (Reference 3) truncated to maximum degree and order 21, or truncated to maximum degree and order 8 (as in GSFC orbit operations), and GEM10B 36 X 36. GEM9 is derived from satellite tracking data, while GEM10B is derived from satellite tracking data, Earth surface gravimetry, and Geodynamics Experimental Ocean Satellite-3 (GEO3-3) altimetry. None of the satellites used in deriving these gravity models had perigee altitudes below 400 kilometers, so that the DE-2 altitudes lie within an altitude range not well covered by the existing GSFC gravity models.

Two atmospheric density models were used and compared, a Harris-Priester model and a Jacchia-Roberts model (Reference 2). The primary difference between these two models, in the context of DE-2 orbit determination, is that the Jacchia-Roberts model attempts to follow transient density effects correlated with the geomagnetic index K_p, while the Harris-Priester model does not use K_p. During periods 1 and 2 geomagnetic activity was low, but during periods 3 and 4 it reached moderate values. The Jacchia-Roberts model was tested only during period 1 in January 1983; definitive Jacchia-Roberts orbit solutions for February 1983 could not be computed because of the lag time in the GTDS data base updates. In all definitive orbit solutions a drag force scale factor, (1 + RHO1), was estimated in addition to the epoch state vector. Solving for this factor nullifies slowly varying systematic differences between atmospheric models and corrects for other constant-factor errors in the drag model, namely, errors in the spacecraft area to mass ratio and the drag coefficient C_D. Changes in the estimated values of RHO1 generally follow changes in the atmospheric density, which are correlated with the Solar 10.7-centimeter specific flux density. This flux density is

plotted in Figure 3 for the periods on study. It is noteworthy that the variations in this flux are generally smooth over periods of several days, and thus the variation of RHO1 in consecutive definitive solutions should be correspondingly smooth for very low-altitude orbits. This smoothness may lead to a short-term predictability in RHO1, increasing the accuracy of short-term, operational orbit predictions.

The spacecraft was model as a sphere for drag force and Solar radiation force modeling, using an area-to-mass ratio of 5.0038×10^{-9} km^2/kg. In the case of the Solar radiation force, the perturbation is very small, anyway, and the error introduced by the sphere approximation is negligible. During the four periods of study, the spacecraft altitude was, for the purpose of drag modeling, constant relative to the orbit, with the cylinder axis oriented perpendicular to both the velocity vector and the orbit plane. Thus, the error of the sphere model relative to a cylinder model is constant with time and this error is corrected by estimation of the drag force scale factor, (1 + RHO1). Hence, the sphere model was adequate in this study.

NASA Spaceflight Tracking and Data Network (STDN) tracking station coordinates (Reference 5) were used in modeling of the tracking observations. These coordinates differ by up to 20 meters in comparison to more accurate coordinates (Reference 6). However, these differences do not significantly affect definitive orbit accuracy until orbit errors are reduced to the 30-meter level, a level well below that encountered in this study. Hence the STDN coordinates were sufficiently accurate for DE-2 orbit determination.

A special version of GTDS was prepared for computation of the solutions that are reported in Sections 4.2.2 and 4.2.3. This version enables the specification and/or estimation of up to eight impulsive forces in an orbit solution. The directions of the impulses could be arbitrarily specified in track-oriented (along-track, cross-track, radial) coordinates. Actually, each impulse could be repeated in a solution an arbitrary number of times at any specified repeat interval; this feature

was used for the results in Section 4.2.2. The formulation used in this study was a mild enhancement of the formulation used in HEAO-2 definitive orbit determination (Reference 1), which was used to model actual, intermittent spacecraft thrusting.

SECTION 3 – ESTIMATES OF DE-2 ORBIT ERRORS

3.1 GRAVITY ERRORS

Since the precise gravity models that are used in orbit determination are expressed in spherical harmonic expansions, it is necessary to have the errors in the expansion coefficients themselves in order to perform orbit error analysis. Since, for example, the GEM10B model contains more than 1000 coefficients, it is clear that simplification in the analysis is necessary. One conventional method of simplification is to use a multiple of the difference between two similar, but uncorrelated, gravity models to estimate the gravity field error in formal orbit error analysis. This approach, containing only one adjustable scale factor, has the advantage of simplicity, but does not directly provide identification of the portions of the model most responsible for the derived orbit errors. At the other extreme, the GSFC Harmonic Analysis Program (HAP) provides very detailed analysis of the sensitivity of an orbit to each of the Fourier components of each spherical harmonic term. This approach give complete resolution but does not explicitly take into account the length of an orbit determination arc (which may be much less than the periods of the perturbations induced by some spherical harmonic terms), nor does it provide a simple means to combine the effects of similar terms.

The approach used here lies between these two extremes. The spherical harmonic terms of the GEM10B model were divided into groups, according to the order m of the terms, $m_1 \leq m \leq m_2$. The effect on an 18-hour DE-2 trajectory resulting from the terms in any one group was directly measured by differencing two trajectories, one trajectory containing this group of terms in the force model and the other trajectory omitting these terms. Assuming linearity, this differencing isolated the effects of the group of terms. Then, the effect of each group was multiplied by an error scale factor that is representative of the error in the harmonic expansion coefficients of each group in order to estimate the orbit error for the group. Of course, the accuracy of the estimate will depend on the accuracy of the error scale factor.

The error scale factors were computed in the following way. Reference 3 provides an error estimate for each term in the GEM10 model. Lower and upper estimates for the error scale factor for each group of terms were computed from the formulas

$$f_1 = \frac{\left[\frac{1}{N}\sum_i \sigma_i^2\right]^{1/2}}{\left[\sum_i (C_i^2 + S_i^2)\right]^{1/2}} \qquad (3\text{-}1)$$

$$f_2 = \frac{\left[\sum_i \sigma_i^2\right]^{1/2}}{\left[\sum_i (C_i^2 + S_i^2)\right]^{1/2}} \qquad (3\text{-}2)$$

where the summations extend over all N terms in a particular group and the σ_i is the error for each pair of coefficients (C_i, S_i) in the group, as tabulated in Reference 3. These error scale factors were based on the GEM10 gravity model, because coefficient errors for the GEM10B model were not readily available. The smaller factor, f_1, would be applicable if all of the coefficient errors in a group were highly correlated with each other, while the larger factor, f_2, applies when the errors in the individual coefficients are independent. At best, these error scale factors merely provide a reasonable range for rough estimates.

The results of this analysis are given in Table 2. Two sets of results are given, one for an 18-hour arc on January 19 and the other for an 18-hour arc on February 12. The maximum perturbations for each group of terms were measured by direct inspection of a plot of the perturbation with time. Generally, orbital frequency oscillations were observed in these plots, within a time-varying envelope and sometimes superimposed on a linear or quadratic secular variation. These secular variations were ignored, since small corrections to the orbital elements or the RHO1 in orbit solutions would compensate for the secular variations. The perturbations tabulated are the largest consecutive maximum to minimum excursions observed at the orbital frequency oscillations, since it was

assumed that the oscillations within the time varying envelopes would not be well-corrected by element or RH01 adjustment.

Overall, the error estimates in Table 2 suggest that the gravity errors in 18-hour DE-2 orbit solutions should be, at most, on the order of 100 to 200 meters. The largest component of the error arises from the near-resonant, m = 16, terms. The orbit errors for these terms are large since most of the satellite orbits used to determine the GEM10B model had resonances with orders 13, 14, or 15, but not 16. It should be noticed that the estimated level of orbit error is only very mildly increased at the later date, seven days prior to re-entry.

3.2 DRAG FORCE ERRORS

Figures 4 and 5 indicate the time variation in the DE-2 drag force. The product of the Harris-Priester model density multiplied by the solved-for value of (1 + RH01) is plotted for several Harris-Priester models for various Solar 10.7-centimeter flux densities. Figure 4 is derived from 18-hour orbit solutions beginning at 0^h on January 19, 1983, while Figure 5 is derived from 18-hour solutions beginning at 0^h on February 12, 1983. The drag force will be nearly proportional to the quantity plotted in these figures since the variation in the square of the spacecraft velocity is small. Figure 4 shows about a 20 to 1 drag variation from perigee to apogee, while Figure 5 shows about a 10 to 1 variation. The Harris-Priester models for large 10.7-centimeter Solar flux densities show smaller perigee-apogee drag variations because the model scale heights are larger than those for lower flux densities.

The drag variations shown in Figures 4 and 5 are, of course, the modelled variations, which are in error to some degree. To improve the drag force modeling, correction of three features is considered in this report. These three features are the following:

(1) Perigee-Apogee Variation. In an orbit solution, this variation is determined by the scale height and diurnal variation in the atmosphere model and by the orbital elements. Correcting

the perigee-apogee variation in each orbit solution assumes that systematic errors exist during the time span of the orbit solution. The detailed shape of the drag variation from perigee to apogee is likely to be of minor importance since this shape is represented by variations occurring on a time scale very much shorter than the orbital period, that is, this shape is represented by high-frequency Fourier components.

(II) Linear Variation in the Overall Level of Drag. As a result of changing orbital elements and the time dependence of the actual atmosphere density, the general level of drag may vary slowly during the timespan of an orbit solution, in a way different than the drag model, and this may require correction.

(III) Random Variations in Atmospheric Density. Transient phenomena in the upper atmosphere, for example, gravity waves, are known to produce 10 to 20 percent changes in the local density. In addition, model errors of 10 to 20 percent, which vary rapidly with position, have been reported for the best atmosphere models (Reference 7). With the type of drag variation that is shown in Figures 4 and 5, random density changes can be approximately modeled as random along-track impulses in the force, positive or negative, occurring at the times of perigee.

In order to estimate the sizes of the orbit position effects resulting from drag variations I and II, the following simplified drag model is introduced. The total along-track drag force, f, is represented by the superposition of a slowly varying term, f_0, and a sinusoidal term of amplitude f_1:

$$f = f_0 + f_1 \cos(\omega_0 t + \phi) \tag{3-3}$$

where ω_0 is the orbital frequency, t is the time, and ϕ is an arbitrary phase. The slowly varying term will be represented as a linear variation:

$$f_0 = a_0 \left[1 + \alpha \frac{\left(t - \frac{T}{2}\right)}{\left(\frac{T}{2}\right)} \right] \tag{3-4}$$

where α is the maximum fractional variation in the drag level and t is the time from the start of a trajectory of duration T. On the basis of elementary linear orbit perturbation theory, the dominant effects of these drag variations can be readily calculated. The dominant along-track effects for the second and fourth periods of study are displayed in Table 3. Note that in this table, the amplitude of the oscillating term is estimated to be equal to the constant term a_0.

Table 3 indicates that for a linear time variation error of 10 percent of the average drag force, the along-track effect is substantial in magnitude, 3.5 or 9.3 kilometers for the two epochs. However, much of the effect varies as t^2 and will be absorbed into estimation of RHO1. Also, much of the t^3 variation will be absorbed by RHO1. For the oscillating component, Table 3 suggests the systematic errors in the oscillation amplitude will lead to marginally important along-track effects. A 10 percent error in the amplitude would lead to 180-meter and 500-meter along-track effects in periods 2 and 4 respectively.

In order to estimate the effects of random drag variations, an impulsive, rather than continuous, model of the drag force is adopted. Drag at apogee is neglected and the peaks near perigee will be approximated as a sequence of delta function impulses, each of strength ΔV_i:

$$f = \sum_{i=1}^{N} \Delta V_i \ \delta(t - t_i) \tag{3-5}$$

where t_i is the time of the i-th perigee. Neglecting periodic effects, linear perturbation theory yields the following estimate for the along-track displacement, $\ell_i(t)$, for the i-th impulse

$$\ell_i(t) = -3 \ \Delta V_i \ g(t - t_i) \tag{3-6}$$

where the function g is defined by

$$\begin{aligned} g(x) &= x \ , \ \text{for } x \geq 0, \\ g(x) &= 0 \ , \ \text{for } x < 0 \end{aligned} \tag{3-7}$$

and where oscillating terms have been omitted.

Equation (3-6) will be used to make numerical estimates. The magnitudes of the ΔV_i can be determined numerically from Figures 4 and 5. Integrating under the F# 150 curves, between the half-maximum points, yields values of 3.3 and 11.5 centimeters per second, respectively, for perigee passages in periods 2 and 4. In order to make precise along-track perturbation estimates, a lengthy, but straight-forward statistical calculation would be required. Rather than attempt this, here it will simply be assumed that a 10 percent error in ΔV occurs for a single impulse at a perigee passage near the middle of an 18-hour trajectory. With this assumption, application of Equation (3-6) yields along-track displacements of 0.3 and 1.1 kilometers, respectively, for periods 2 and 4. From these estimates, it is clear that random fluctuations in the drag force can lead to significant orbit solution errors for DE-2, when errors from several perigee passages are superimposed.

SECTION 4 – RESULTS

4.1 ORBIT DETERMINATION USING STANDARD METHODS

4.1.1 EFFECT OF GRAVITY MODEL

Three sets of orbit solutions were computed, one set using the GEM9 8 X 8 gravity model and the F# 150 Harris-Priester model, one set using the GEM9 21 X 21 gravity model and the F# 225 Harris-Priester model, and one set using the GEM10 36 X 36 gravity model and the F# 225 Harris-Priester model. The RMS weighted residuals for these solutions are shown in Table 4. For periods 1 and 2, much better fits to the tracking data are obtained as the gravity model is improved, but this trend is not observed in periods 3 and 4.

The 6-hour solution overlap differences are shown in Table 5. Mild reductions in the overlap differences are found for periods 1 and 2 (although these reductions are not as strong as the reductions in the RMS weighted residuals) but no consistent trends are observed in periods 3 and 4.

Comparisons between the 18-hour GEM9 8 X 8 solutions and the corresponding GEM10B solutions yielded maximum position differences which were typically 200 to 300 meters in period 1 and 400 to 600 meters in period 2.

The natural interpretation of these results is that gravity errors are significant in periods 1 and 2, but in periods 3 and 4, drag errors are very much larger than gravity errors, making gravity improvements undiscernable in the results. The overlap differences observed in periods 1 and 2 are consistent with the gravity error estimate of 100 to 200 meters in Section 3.1: evidently, solutions in these two periods contain a comparable amount of drag error.

4.1.2 EFFECT OF ATMOSPHERIC DENSITY MODEL

Four sets of GEM10B 36 X 36 orbit solutions were calculated, one set in period 1 using the Jacchia-Roberts model, and three complete sets using the F# 75, F# 150, and F# 225 Harris-Priesters. As

with all orbit solutions for this report, RHO1 was solved for in each individual solution. As indicated by Figures 4 and 5, the primary effect, on short orbit solutions, of varying the F# is to change the atmosphere scale height and, hence, to perigee-apogee variation in the drag force. The Jacchia-Roberts model introduces time dependence into the model density, but these effects are expected to be small for period 1.

The RMS weighted residuals for these solutions are shown in Table 6 and the solution overlap comparisons are given in Table 7. The solutions in periods 1 and 2 show a slightly better fit with the F# 150 Harris-Priester model. This value for the Solar flux is near the actual values for these periods. (See Figure 3.) A preference for the actual values of the Solar flux is not evident in periods 3 and 4. The overlap differences in Table 7, except for period 4, roughly match the trends in the RMS weighted residuals. Typical differences between Jacchia-Roberts and Harris-Priester solutions were 100 to 300 meters. Typical differences between corresponding Harris-Priester solutions of different flux numbers were 100 to 200 meters in period 1 and 400 to 800 meters in period 4.

As in many other orbit accuracy studies, the more complex Jacchia-Roberts model does not yield more accurate orbit solutions.

4.1.3 EFFECT OF LENGTH OF ORBIT SOLUTION

In operational GSFC orbit determination for DE-2, the lengths of orbit solutions were generally about 32 hours long, with 8-hour overlaps, except during the last two weeks, when shorter solutions were computed. Operational solutions used the GEM9 8 × 8 gravity model with estimation of RHO1 in each solution.

The effects of the longer solution length are shown in Table 8. As expected, both the RMS weighted residuals and the overlap differences are substantially higher for the 32-hour solutions; the RMS weighted residuals are about a factor of two larger, while the increase in the overlap differences is not quite so large.

4.2 ORBIT DETERMINATION USING FORCE MODEL ADJUSTMENT

4.2.1 ADJUSTMENT OF THE LINEARLY VARYING DRAG SCALE FACTOR

In these solutions an attempt was made to correct for systematic changes in the drag force level, which may possibly occur during the period covered by an orbit solution. This is variation II described in Section 3.2. Eight parameters were solved for in each solution, six orbital elements and two coefficients in a linear polynomial for RHO1. This capability is available in the standard version of GTDS.

A summary of these solutions is shown in Table 9. Compared with corresponding solutions in which only a constant RHO1 was estimated (Tables 4 and 5), these solutions show a much better fit to the tracking data, particularly in period 4. However, the period 2 overlap differences were not improved and the period 4 overlap differences became an order of magnitude larger. The behavior observed in period 4 was also noted in the HEAO-2 study. In Table 9, the solved-for values of RHO1 at the starting times and ending times of consecutive solutions show some degree of continuity, but there are glaring exceptions, indicating that the technique is responding to errors that are not linearly varying drag errors.

Empirically, the procedure of solving for the linearly varying drag factor has performed very poorly in a time period, period 4, in which it might be thought to be most useful. This may be related to the fact that each solution contained only, typically, eight passes of tracking.

4.2.2 ADJUSTMENT OF THE PERIGEE-APOGEE DRAG VARIATION

In these solutions the ratio of the drag force at perigee to the drag force at apogee was adjusted, in addition to the drag force parameter RHO1. This is variation I in Section 3.2.1. A special version of GTDS was used for these calculations. At each apogee, an along-track impulse was applied and estimated, the same impulse at each apogee. For these eight-parameter solutions the GEM10B 36 X 36 model and the F=150 Harris-Priester model were used.

These solutions are summarized in Table 10. Compared to corresponding results in Tables 6 and 7, the fit to the tracking data is not much changed in period 1, but moderately improved in period 2. However, as judged by the solution overlap differences, estimation of the accuracy did not improve the solution accuracies, overall. The strengths of the estimated impulses are given in Table 10; these are about 10 percent and 7 percent of the perigee drag effects in periods 1 and 4 respectively. Also, Table 10 indicates that the new solve-for parameter is strongly correlated with the RHO1 solve-for parameter, although not strongly enough to damage the numerical accuracy of the solutions.

The results suggest that, although the perigee-apogee drag variation should be a parameter with a significant effect on DE-2 solution accuracy, it is probably not the largest error source and reduction of some other error must first be obtained before correction of this effect can become significant.

4.2.3 ADJUSTMENT OF RANDOM DRAG FORCES

Here, an attempt was made to estimate, at least partially, some of the random variations in the drag force, variation III described in Section 3.2. To accomplish this, along-track impulses were placed at selected perigee points in each solution, and the magnitudes of these impulses were individually estimated, along with RHO1 and the orbital elements in each solution. For periods 1 and 2, solutions having one, two, three, and four estimated impulses were calculated. All of the solutions included the GEM10B 36 X 36 model and the F# 150 Harris-Priester model.

An 18-hour solution contains about 12 DE-2 perigee passages. It is clear, that with the amount of tracking available (Table 4), an impulse at each perigee passage cannot be estimated. Furthermore, since data is not available between all consecutive perigees, impulses between distinct perigees may not be distinguishable in orbit solutions. In this pilot study, the impulses were placed so as to divide each solution into roughly equal segments, taking care to ensure the presence of tracking data between estimated impulses.

The RMS weighted residuals are shown in Table 11. A clear, strong decrease as more impulses are added is observed. (The RMS weighted residuals for a particular case may increase as more impulses are added, because the impulses are added at different perigee passages.) Table 12 shows the overlap differences. Compared to the corresponding differences in Table 7, period 1 differences with impulses show a mild decrease, consistent with the estimate of 100 to 200 meters of gravity error. However, the overlap differences for period 4 show a much larger improvement, from 1100 meters to about 500 meters.

The sizes of the estimated impulses are shown in Table 13. The average magnitudes (disregarding the sign) are also given. These averages are physically reasonable. In period 1 the averages range from 19 to 26 percent of the average perigee drag impulse, and for period 4 the averages range from 10 to 22 percent of the total. Surprisingly, there was no difficulty is estimating ten or eleven parameters with the available tracking data. Table 14 shows the correlation coefficients for the three-impulse solutions of period 4. Even though each of these solutions contained about eight passes of tracking, the largest correlation coefficient among the solved-for impulses and RHO1 was 0.97, and typically much smaller.

Differences between corresponding solutions calculated with and without impulses were typically 100 to 300 meters during period 1 and 500 to 1500 meters during period 4.

4.3 ORBIT PREDICTION

Operational orbit prediction is concerned with prediction periods of, typically, five days. For DE-2, the major factor controlling prediction error is the magnitude of the average drag force; errors in this cause along-track prediction errors to grow as the square of the elapsed time. This will outgrow effects of errors in the elements, which lead to along-track error growth which is proportional to the elapsed time. In addition, gravitational resonance effects for DE-2 are small for the periods

considered here. Hence, prediction accuracy will depend crucially on the value of the drag scale factor (1 + RHO1) used in the prediction.

For predictions in periods 1 and 2, two types of predicted values for RHO1 are considered, constant values and linearly varying values.

4.3.1 CONSTANT DRAG SCALE FACTOR

Current GSFC operational orbit prediction procedures use the last value of RHO1 obtained in definitive solutions for the predicted orbit. This procedure was followed to obtain the results in Tables 15 and 16. A different value of RHO1 was used in each prediction, obtained from the corresponding definitive solution. The results in Table 15 were obtained using initial elements and RHO1 values from GEM9 21 X 21 definitive solutions, while the results in Table 16 correspondingly used GEM9 8 X 8 definitive solutions.

The prediction accuracies are about the same, typically 200 kilometers after five days, regardless of the gravity model.

In order to further study the effects of the predictive value of RHO1, an additional set of predictions was computed. Here, the average value of RHO1 during the prediction interval was used. This average value was obtained from existing definitive solutions within the prediction interval. Of course, this could not be an operational procedure, but this test was performed to determine whether an average value of RHO1 would lead to better prediction accuracy.

The results of this test are shown in Table 17. The five-day prediction error was observed to increase slightly, relative to the errors in Tables 16 and 17. This is probably the result of errors building up early during the prediction period for the predictions using the average RHO1.

4.3.2 LINEARLY VARYING DRAG SCALE FACTOR

The results just described indicated the need for more accurate RHO1 values in prediction. More accurate values were provided by the sectioned, linear approximation shown in Figure 6. This linear approximation was simply an eye fit to the definitive values of RHO1 obtained for period 1 and period 2 solutions. The capability to include a sectioned, linear RHO1 approximation is included in the current operational version of GTDS.

The prediction errors obtained using the sectioned linear approximation are given in Table 18. The increase in accuracy is marked; five-day prediction errors have been reduced from the 200-kilometer level to the 20-kilometer level. These results show that orbit prediction accuracy can be substantially increased provided good linear predictions of RHO1 can be made. RHO1 tends to follow the Solar 10.7-centimeter flux density and as indicated in Section 2, this flux density varies smoothly over five- to 20-day periods, so that RHO1 may be predictable. Further study of this question is required.

SECTION 5 – CONCLUSION

Definitive orbit determination accuracy levels for DE-2 were established. For the slightly elliptical orbit, ranging from 230 to 380 kilometers altitude, an accuracy level of 200 to 300 meters was obtained using the GEM10B gravity model in 18-hour solutions. In the altitude range 190 to 270 kilometers, accuracies of about 1000 to 1500 meters were obtained. These accuracies were derived using standard gravity and atmosphere models. In the latter case, atmospheric drag errors appeared to form most of the total error. For both altitude ranges, the accuracy levels obtained using a much less precise GEM9 8 X 8 gravity model were similar to the GEM10B accuracies.

A technique for estimating random drag force errors was tested. At the lowest altitude range, the technique significantly improved the quality of the fit to the tracking data and appeared also to substantially improve the solution accuracies. The application of this technique was limited by the availability of tracking passes; with approximately 20 passes of ground tracking data per day, or equivalent amounts of Tracking Data Relay Satellite System (TDRSS) data, this technique could be more fully tested.

The DE-2 orbit prediction study showed that improvement in low-altitude orbit prediction reduces, essentially, to prediction of the drag force scale adjustment parameter RHO1. Substantial improvements in orbit prediction accuracy were shown to be possible if good, piecewise-linear predictions of RHO1 can be made for periods of five to ten days. The predictability of RHO1 in operational orbit determination is suggested as a question for future study.

REFERENCES

1. Computer Sciences Corporation, CSC/TM-82/6163, *Definitive Orbit Determination for the HEAO-2 Spacecraft*, R. L. Smith and M. K. Mallick, November 1982.

2. Goddard Space Flight Center, X-582-76-77, *Mathematical Theory of the Goddard Trajectory Determination System*, J. O. Capellari, Jr., C. E. Velez, and A. J. Fuchs (editors), April 1976.

3. F. J. Lerch, S. M. Klosko, R. E. Laubsher, and C. A. Wagner, "Gravity Model Improvement Using GEOS-3 (GEM9 and GEM10)," *Journal of Geophysical Research*, Volume 84, p. 3897, 1979.

4. F. J. Lerch, C. A. Wagner, S. M. Klosko, and B. H. Putney, "Goddard Earth Models for Oceanographic Applications (GEM10B and 10C)," *Marine Geodesy*, Volume 5, Number 2, p. 145, 1981.

5. National Aeronautics and Space Administration, *NASA Directory of Station Locations*, Fourth Edition, February 1978.

6. J. G. Marsh, R. G. Williamson, and T. V. Martin, "Tracking Station Coordinate Investigation," paper presented at the GEOS-3 Principal Investigators Meeting, NASA GEOS-3 Project, New Orleans, Louisiana, November 1977.

7. U. von Zahn and K. H. Fricke, "Empirical Models of Global Thermospheric Composition and Temperature During Geomagnetically Quiet Times Compared With Esro 4 Gas Analyzer Data," *Reviews of Geophysics and Space Science*, Volume 16, Number 2, May 1978.

FIGURE CAPTIONS

Figure 1. Altitude History of DE-2 Before Re-entry.

Figure 2. DE-2 Tracking Data Distribution Before Re-entry.

Figure 3. 10.7-Centimeter Solar Flux Density During DE-2 Orbit Determination Periods.

Figure 4. Variation in DE-2 Drag Force for Period 2.

Figure 5. Variation in DE-2 Drag Force for Period 4.

Figure 6. DE-2 Definitive Values of RHO1 and the Sectioned Linear Approximation Used in Prediction.

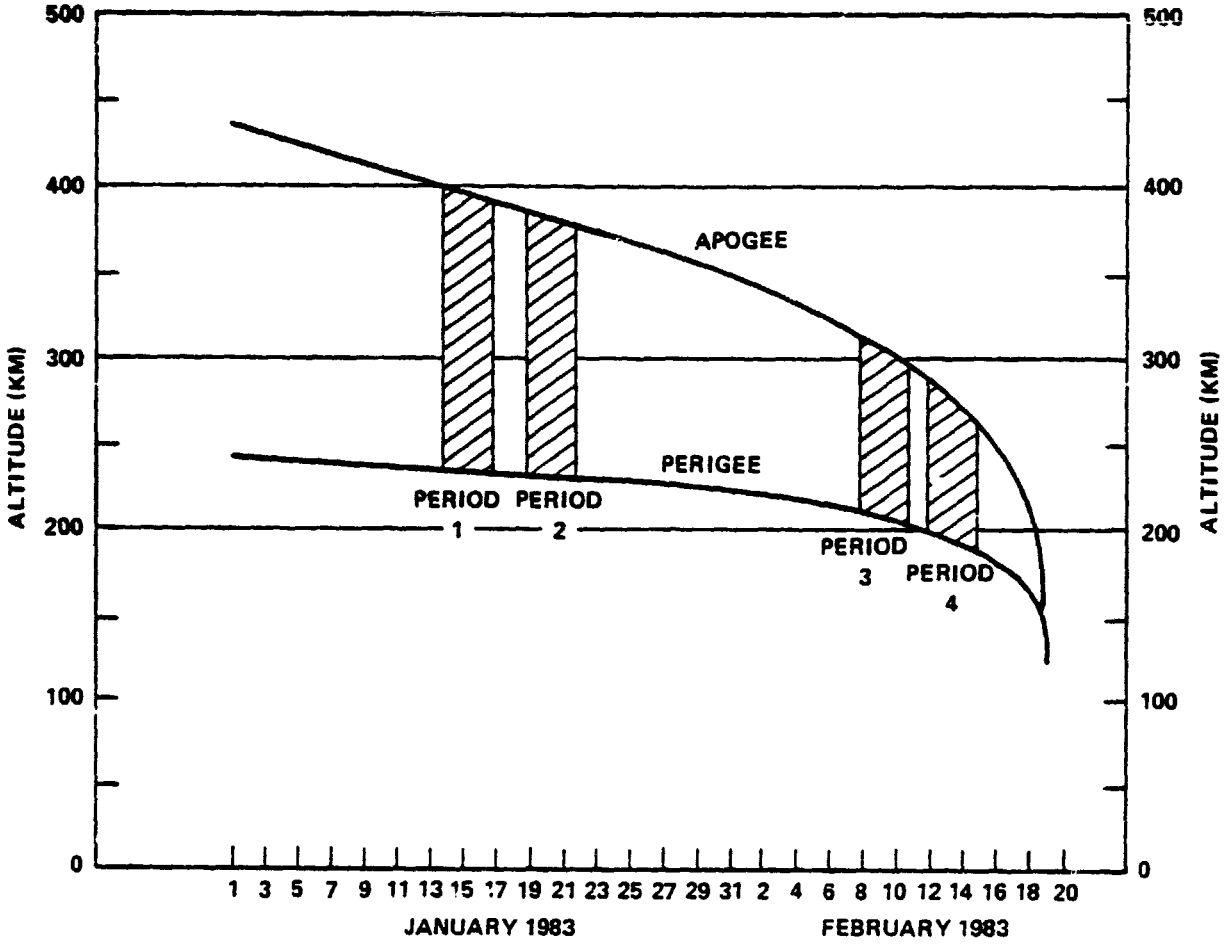

Figure 1. Altitude History of DE-2 Before Re-entry.

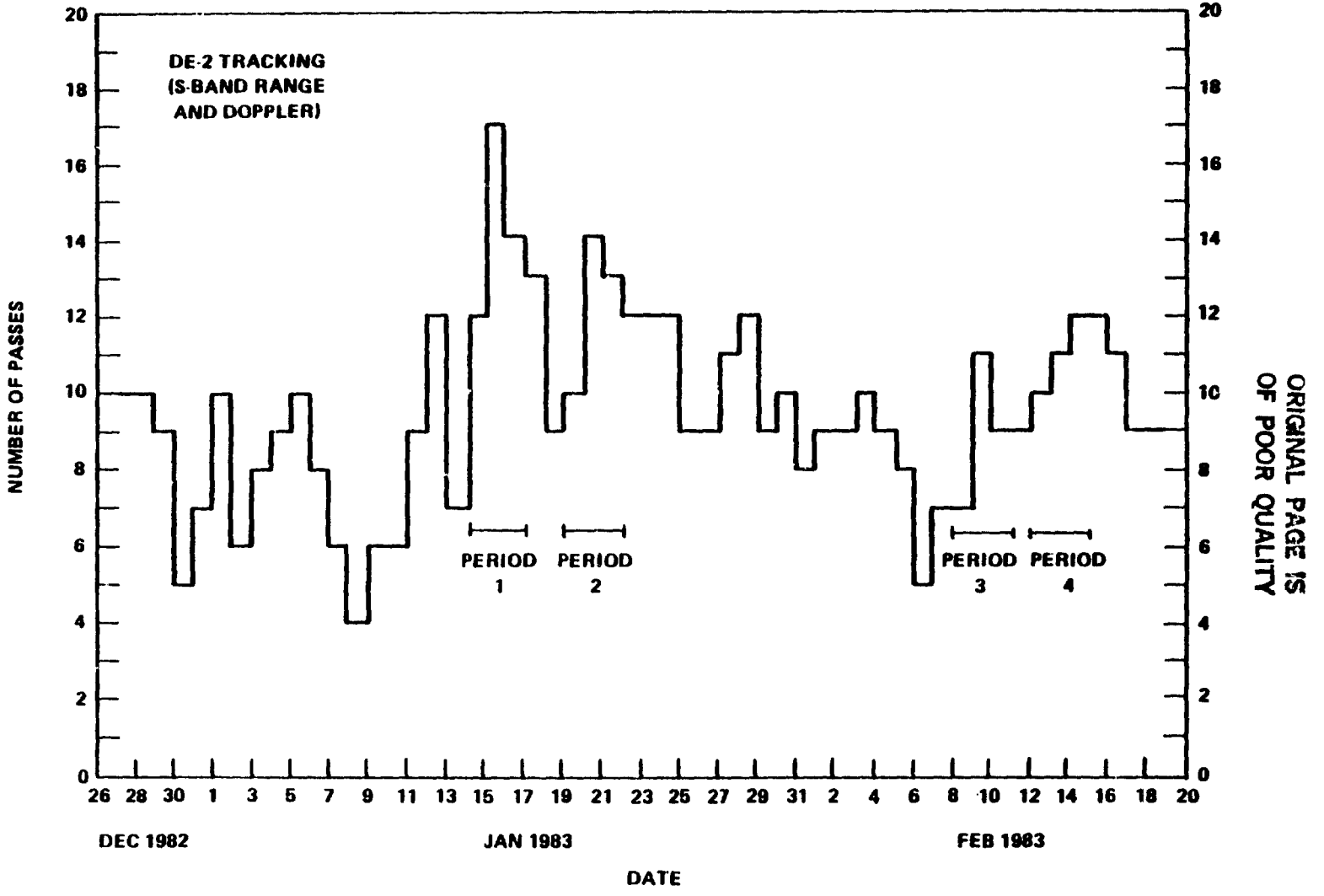

Figure 2. DE-2 Tracking Data Distribution Before Re-entry.

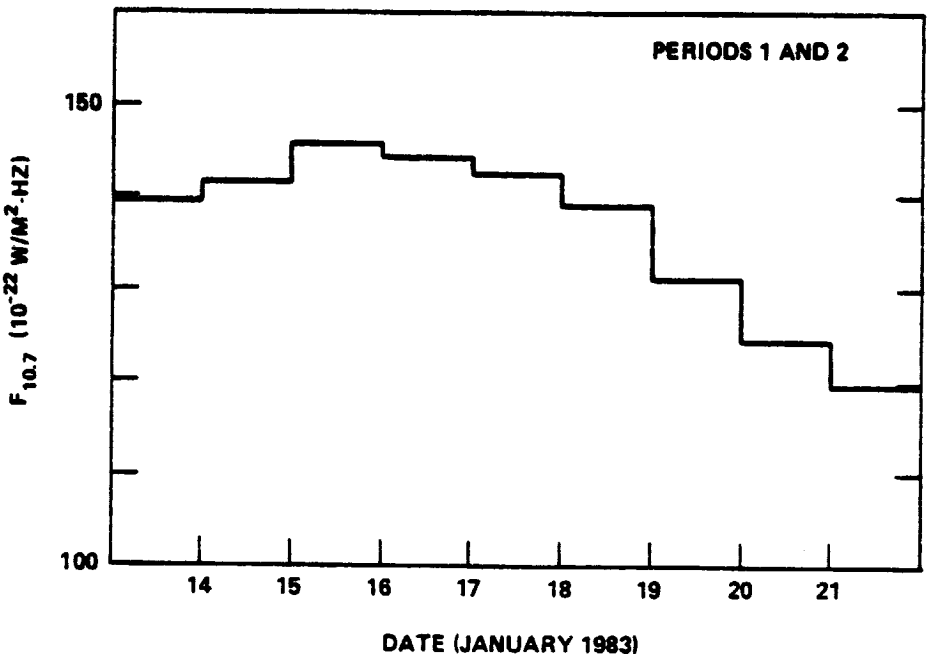

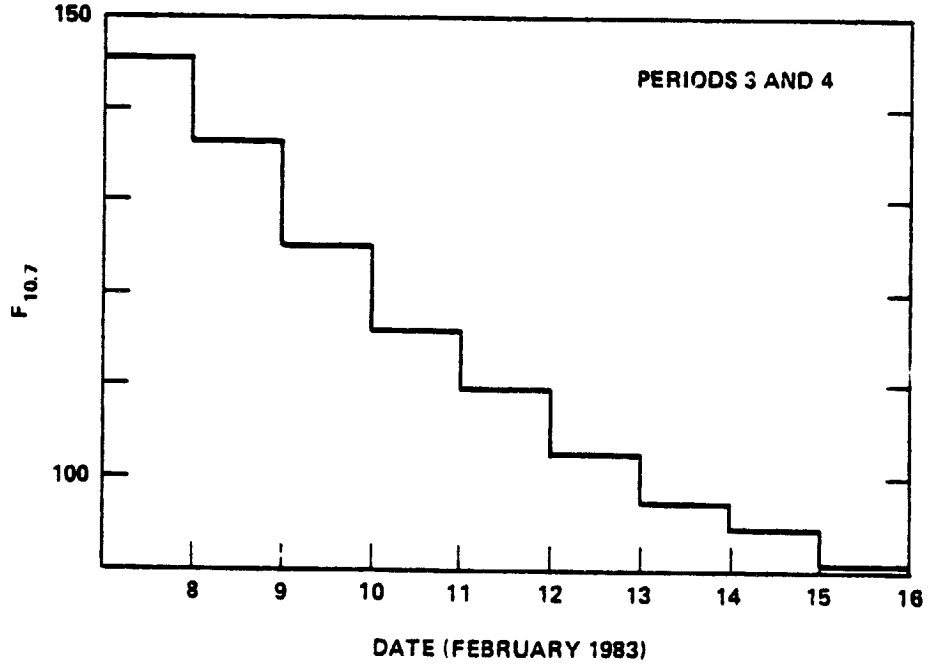

Figure 3. 10.7-Centimeter Solar Flux Density During DE-2 Orbit Determination Periods.

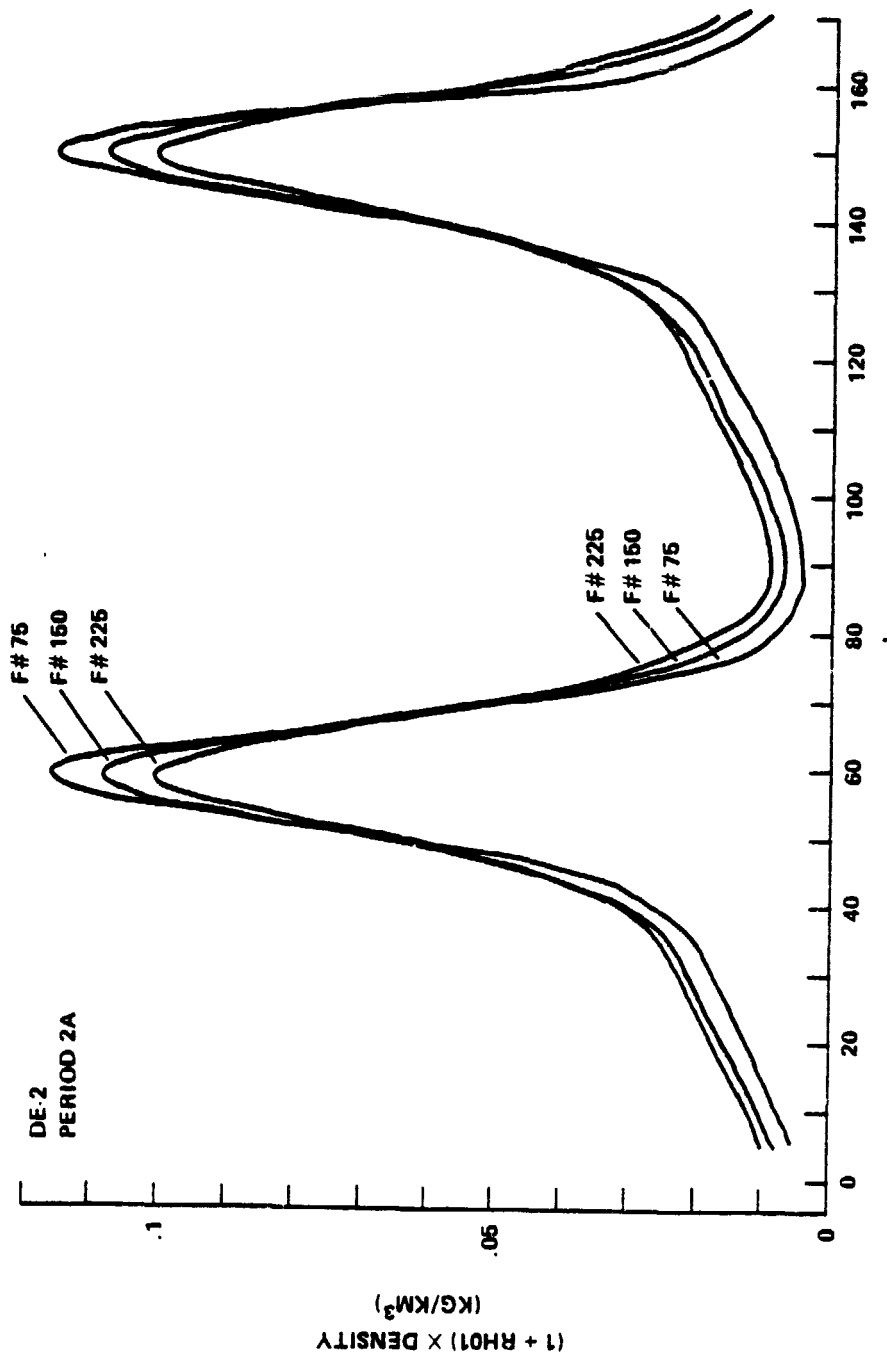

Figure 4. Variation in DE-2 Drag Force for Period 2.

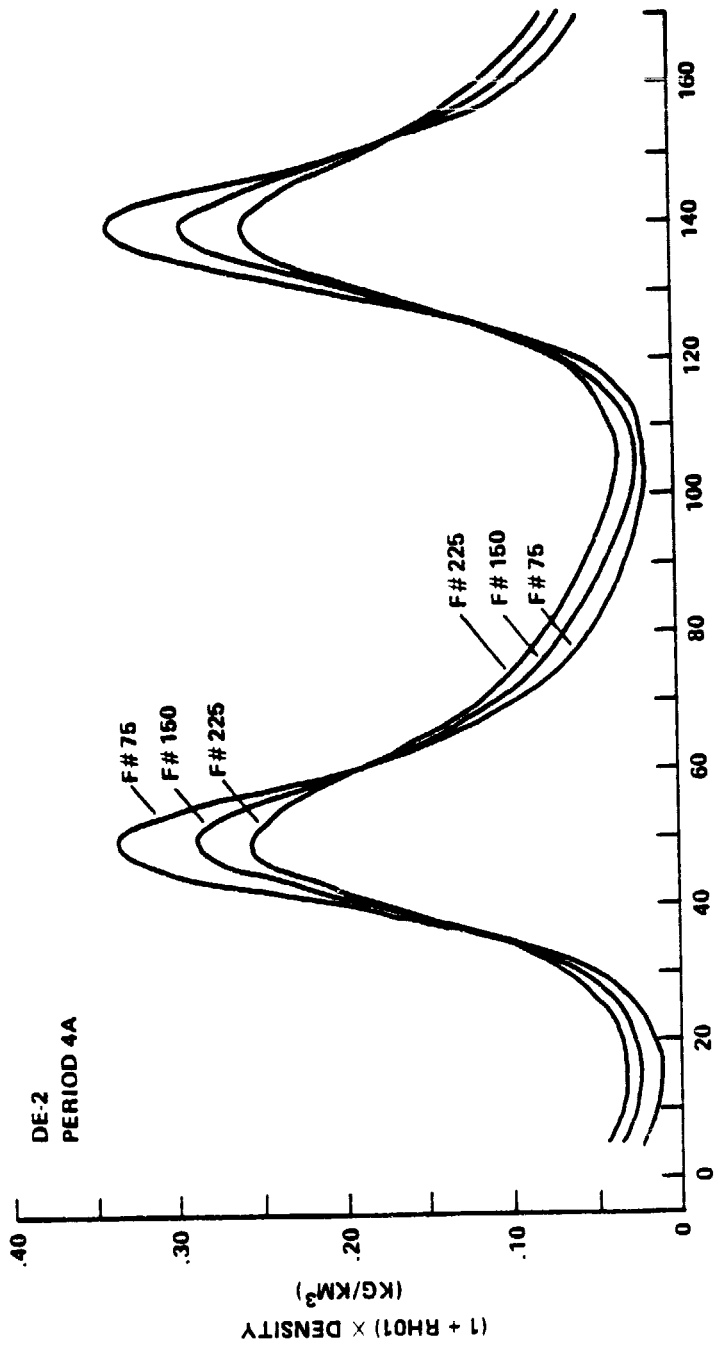

Figure 5. Variation in DE-2 Drag Force for Period 4.

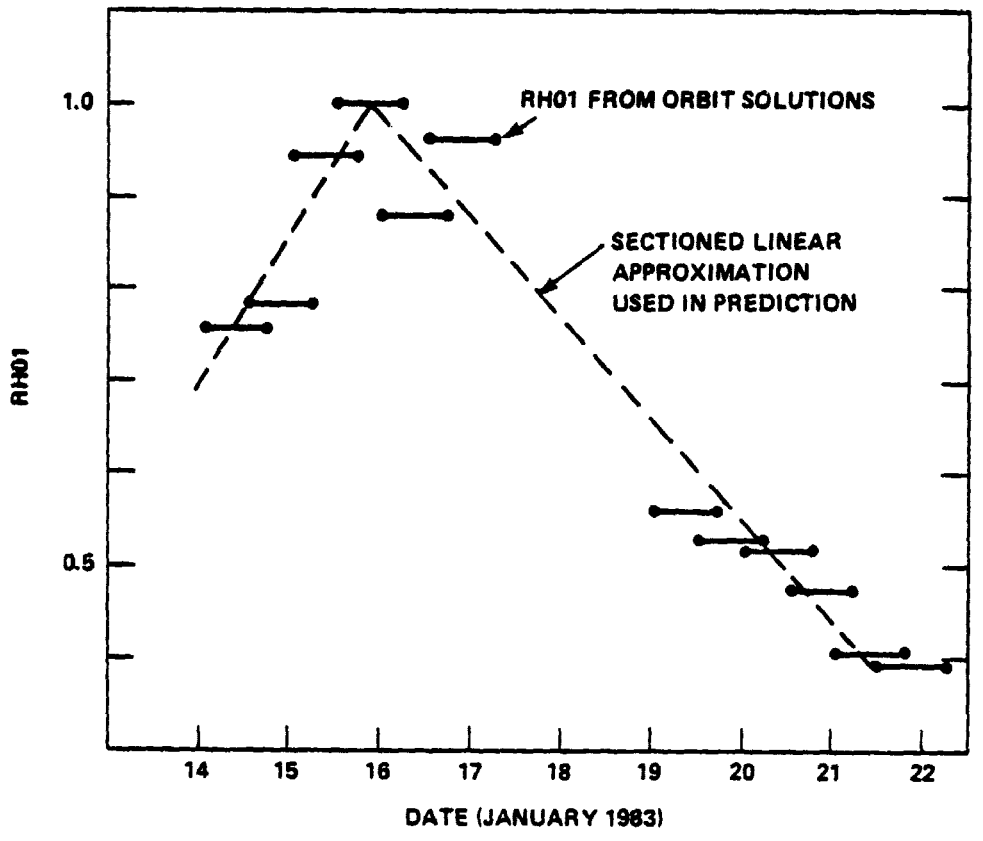

Figure 6. DE-2 Definitive Values of RHO1 and the Sectioned Linear Approximation Used in Prediction.

TABLE CAPTIONS

Table 1. Osculating Keplerian Orbital Elements for DE-2.

Table 2. Gravity Error Analysis for DE-2.

Table 3. Estimates of Drag Effects for DE-2.

Table 4. RMS Weighted Residuals from DE-2 Orbit Solutions (Gravity Model Varied).

Table 5. Ephemeris Differences Between Overlapping DE-2 Orbit Solutions (Gravity Model Varied).

Table 6. RMS Weighted Residuals for DE-2 Orbit Solutions (Atmosphere Model Varied).

Table 7. Ephemeris Differences Between Overlapping DE-2 Orbit Solutions (Atmosphere Model Varied).

Table 8. Comparison of 18-Hour and 32-Hour Orbit Solutions for DE-2.

Table 9. Summary of DE-2 Orbit Solutions Including Estimation of a Linearly-Varying Drag Scale Factor.

Table 10. Summary of DE-2 Orbit Solutions in Which the Perigee-Apogee Drag Variation Was Estimated.

Table 11. RMS Weighted Residuals for DE-2 Orbit Solutions That Included Estimation of Random Drag Forces.

Table 12. Ephemeris Differences Between Overlapping DE-2 Orbit Solutions That Included Estimation of Random Drag Forces.

TABLE CAPTIONS (Continued)

Table 13. Solved-for Values of Along-Track Impulses Placed At Selected Perigee Points in DE-2 Orbit Solutions.

Table 14. Correlation Coefficients from a DE-2 Orbit Solutions in Which Three Perigee Impulses Were Estimated.

Table 15. DE-2 Prediction Accuracy Using the Last Definitive Values of RHO1 (GEM9 21 X 21).

Table 16. DE-2 Prediction Accuracy Using the Last Definitive Values of RHO1 (GEM9 8 X 8).

Table 17. DE-2 Prediction Accuracy Using the Average Value of RHO1 for the Prediction Interval.

Table 18. DE-2 Prediction Accuracy Using a Sectioned Linearly Varying Value of RHO1 in the Prediction Interval.

Table 1
Osculating Keplerian Orbital Elements for DE-2

Orbital Element	Epoch	
	0^h January 14, 1983	0^h February 12, 1983
Semimajor Axis (km)	6693.3	6631.9
Eccentricity	0.0112	0.0054
Inclination (Degrees)	89.99	89.92
Argument of Perigee (Degrees)	3.89	233.03
Right Ascension of Ascending Node (Degrees)	157.98	158.08
Mean Anomaly (Degrees)	45.41	136.07

Table 2
Gravity Error Analysis for DE-2

Group Order Limits		Maximum Position Perturbation (M)			Error Scale Factors		Orbit Error Estimates (M)		
M1	M2	Radial	Cross-Track	Along-Track	f_1	f_2	Radial	Cross-Track	Along-Track
Epoch: Jan 19, 1983									
0*	0*	1050	5	2000	0.004	0.02	4 to 20	0 to 1	8 to 40
1	1	320	720	990	0.004	0.02	1 to 6	3 to 14	4 to 20
2	2	720	680	2400	0.003	0.02	2 to 14	2 to 14	7 to 48
3	4	200	340	600	0.006	0.04	1 to 8	2 to 14	4 to 24
5	15	160	130	430	0.008	0.10	1 to 16	1 to 13	3 to 43
16	16	130	80	290	0.10	0.40	13 to 52	8 to 32	29 to 116
17	36	40	65	140	0.01	0.06	0 to 2	1 to 4	1 to 8
Epoch: Feb 12, 1983									
0*	0*	1300	5	2500	0.004	0.02	5 to 26	0 to 1	10 to 50
1	1	220	760	800	0.004	0.02	1 to 4	3 to 15	3 to 16
2	2	800	800	2400	0.003	0.02	2 to 16	2 to 16	7 to 48
3	4	200	140	1000	0.006	0.04	1 to 8	1 to 6	8 to 56
5	15	150	130	1400	0.008	0.10	1 to 15	1 to 13	11 to 140
16	16	80	120	180	0.10	0.40	8 to 32	12 to 48	18 to 72
17	36	45	100	160	0.01	0.06	0 to 3	1 to 6	2 to 10

*Degree > 2

Table 3
Estimates of Drag Effects for DE-2

Type of Drag Variation	Dominant Along-Track Effect	Maximum Along-Track Position Variation* (km)	
		January 19, 1983	February 12, 1983
Constant a_0	$\frac{3}{2} a_0 t^2$	100.	280.
Linear in Time $\alpha a_0 \frac{\left(t-\frac{T}{2}\right)}{\left(\frac{T}{2}\right)}$	$\alpha a_0 t^2 \frac{\left(\frac{3}{2} T-t\right)}{T}$	0.35 (for $\alpha = 0.01$)	0.93 (for $\alpha = 0.01$)
Oscillating $a_0 \cos(\omega_0 t + \phi)$	$\frac{2 a_0 t}{\omega_0} \sin(\omega_0 t + \phi)$	1.8	5.0

*For 18-hour propagations.

Table 4
RMS Weighted Residuals from DE-2 Orbit Solutions
(Gravity Model Varied)

Solution Interval*	Passes of Tracking	RMS Weighted Residual		
		GEM9 8 X 8	GEM9 21 X 21	GEM10B 36 X 36
1A	10	16.6	9.5	8.0
1B	8	8.1	8.2	4.6
1C	9	12.0	11.2	8.2
1D	15	19.4	9.0	6.6
1E	11	11.4	12.1	13.1
1F	10	17.7	20.0	15.5
	Averages:	14.2	11.7	9.3
2A	7	–	7.6	2.9
2B	9	–	10.4	7.0
2C	9	–	11.3	7.5
2D	10	–	11.4	11.3
2E	10	–	10.5	5.4
2F	11	–	9.1	5.0
	Averages:		10.1	6.5
3A	5	–	3.7	2.0
3B	6	–	12.7	9.3
3C	7	–	21.9	22.6
3D	7	–	26.2	32.0
3E	6	–	7.8	7.1
3F	5	–	12.3	9.6
	Averages:		14.1	13.8
4A	8	46.3	30.3	41.5
4B	9	61.4	48.7	47.5
4C	8	25.5	14.0	17.8
4D	8	21.8	31.4	30.9
4E	8	19.8	19.8	24.9
4F	8	17.6	17.9	15.8
	Averages:	32.1	27.0	29.7

*Consecutive, overlapping orbit solutions are identified by a two-character label. The first character indicates the period number and the second character indicates the relative position of the solution within the period.

Table 5
Ephemeris Differences Between Overlapping DE-2 Orbit Solutions
(Gravity Model Varied)

Comparison Interval	Maximum Overlap Difference (Meters)		
	GEM9 8 X 8	GEM9 21 X 21	GEM10B 36 X 36
1A-1B*	400	422	293
1B-1C	264	342	320
1C-1D	417	224	250
1D-1E	161	206	260
1E-1F	327	348	306
Averages:	314	308	286
2A-2B	–	361	257
2B-2C	–	269	211
2C-2D	–	750	449
2D-2E	–	234	287
2E-2F	–	236	135
Averages:		370	268
3A-3B	–	702	856
3B-3C	–	531	440
3C-3D	–	1506	1285
3D-3E	–	381	419
3E-3F	–	897	650
Averages:		803	730
4A-4B	1489	2134	2083
4B-4C	825	534	564
4C-4D	912	1330	1508
4D-4E	1639	1710	1612
4E-4F	831	1768	[illegible]
Averages:	1139	1495	1508

*Indicates that solution 1A is compared with solution 1B in the overlap interval.

Table 6
RMS Weighted Residuals for DE-2 Orbit Solutions
(Atmosphere Model Varied)

Solution Interval*	RMS Weighted Residual			
	Jacchia-Roberts	Harris-Priester F# 75	Harris-Priester F# 150	Harris-Priester F# 225
1A	6.8	6.7	6.2	8.0
1B	5.4	8.0	4.2	4.6
1C	11.8	5.4	5.2	8.2
1D	16.1	13.3	5.6	6.6
1E	12.6	8.0	12.2	13.1
1F	9.0	17.4	13.9	15.5
Averages:	[illegible].3	9.8	7.9	9.3
2A	–	4.1	2.6	2.9
2B	–	6.2	6.2	7.0
2C	–	5.3	6.2	7.5
2D	–	10.2	10.5	11.3
2E	–	4.6	4.2	5.4
2F	–	6.2	4.5	5.0
Averages:		6.1	5.7	6.5
3A	–	8.9	3.1	2.0
3B	–	7.7	5.5	9.3
3C	–	22.8	21.1	22.6
3D	–	38.1	34.8	32.0
3E	–	15.3	8.7	7.1
3F	–	14.6	8.9	9.6
Averages:		17.9	13.7	13.8
4A	–	69.2	52.4	41.5
4B	–	51.2	45.9	47.5
4C	–	45.1	18.8	17.8
4D	–	36.0	16.3	31.0
4E	–	33.5	6.6	25.0
4F	–	55.4	30.5	15.8
Averages:		48.4	28.4	29.8

*See Table 4 footnote.

Table 7
Ephemeris Differences Between Overlapping DE-2 Orbit Solutions
(Atmosphere Model Varied)

Comparison Interval*	Maximum Overlap Differences (Meters)			
	Jacchia-Roberts	Harris-Priester F# 75	Harris-Priester F# 150	Harris-Priester F# 225
1A-1B	202	126	158	293
1B-1C	194	266	191	320
1C-1D	567	188	228	250
1D-1E	272	322	160	260
1E-1F	169	604	189	306
Averages:	281	301	185	286
2A-2B	–	331	174	257
2B-2C	–	57	113	211
2C-2D	–	376	349	449
2D-2E	–	287	266	287
2E-2F	–	77	78	135
Averages:		226	196	268
3A-3B	–	985	700	856
3B-3C	–	808	597	440
3C-3D	–	1092	498	1285
3D-3E	–	1150	731	419
3E-3F	–	1007	260	650
Averages:		1008	557	730
4A-4B	–	1999	1817	2083
4B-4C	–	1771	752	564
4C-4D	–	1088	1048	1508
4D-4E	–	1568	692	1612
4E-4F	–	1393	1368	1774
Averages:		1564	1135	1508

*See Table 5 footnote.

Table 8
Comparison of 18-Hour and 32-Hour Orbit Solutions for DE-2

Solution Epoch (1983)	Passes of Tracking	RMS Weighted Residual	Maximum Overlap Difference (Meters)
18-Hour Solutions			
Jan 14, 0^h	10	16.6	400
Jan 14, 12^h	8	8.1	264
Jan 15, 0^h	9	12.0	417
Jan 15, 12^h	15	19.4	161
Jan 16, 0^h	11	11.4	327
Jan 16, 12^h	10	17.7	–
		Averages: 14.2	314
32-Hour Solutions			
Jan 14, 0^h	18	30.8	669
Jan 15, 0^h	20	30.2	408
Jan 16, 0^h	18	28.7	–
		Averages: 29.9	539

Note: All solutions used the GEM9 8 X 8 gravity model.

Table 9
Summary of DE-2 Orbit Solutions Including Estimation
of a Linearly-Varying Drag Scale Factor

Solution Interval	RMS Weighted Residual	Maximum Overlap Difference (Meters)	Drag Scale Factor*	
			Start	End
1A	7.3	139	.081	.017
1B	4.5	367	.059	.071
1C	6.3	273	.105	.215
1D	6.5	453	.188	.201
1E	13.0	395	.129	.112
1F	9.2	—	.301	.064
Averages:	7.8	325		
4A	20.3	12809	.040	.226
4B	14.2	8869	.291	.169
4C	15.2	6103	.141	.207
4D	18.2	17625	.307	.087
4E	11.8	9958	.049	.165
4F	15.4	—	.164	.177
Averages:	15.9	11073		

*A linearly-varying RHO1 was estimated in each 18-hour solution. The values tabulated correspond to the start and end of each solution. The GEM10B 36 × 36 gravity model and the F=225 Harris-Priester model were used for solutions in this table.

Table 10
Summary of DE-2 Orbit Solutions in Which the Perigee-Apogee Drag Variation Was Estimated

Solution Interval	RMS Weighted Residual	Maximum Overlap Difference (Meters)	Impulse Strength (cm/s)	Correlation Coefficient*
1A	5.0	151	0.24	.993
1B	3.9	19	−0.81	.996
1C	4.3	171	0.15	.988
1D	5.0	178	0.15	.996
1E	11.3	367	0.30	.997
1F	13.1	–	0.23	.987
Averages:	7.1	208	0.31	
4A	30.4	1367	−1.40	.977
4B	33.2	602	1.29	.992
4C	11.5	1121	−0.52	.986
4D	15.9	696	−0.14	.983
4E	6.6	1719	−0.25	.946
4F	16.7	–	−1.10	.985
Averages:	19.1	1101	0.78	

*Between RH01 and the impulse strength.

Table 11
RMS Weighted Residuals for DE-2 Orbit Solutions That Included Estimation of Random Drag Forces

Solution Interval*	RMS Weighted Residual			
	One Impulse	Two Impulses	Three Impulses	Four Impulses
1A	6.2	5.3	4.6	3.8
1B	3.9	3.4	3.3	0.9
1C	4.7	1.8	2.1	1.9
1D	4.9	4.5	4.5	3.7
1E	9.3	9.8	4.4	3.7
1F	13.4	4.5	4.6	2.9
Averages:	7.1	4.9	3.9	2.8
4A	47.5	13.5	6.6	3.0
4B	42.0	17.5	12.5	9.6
4C	18.6	7.9	14.7	5.2
4D	10.8	12.2	7.1	5.5
4E	5.5	5.8	5.4	5.2
4F	28.7	18.2	11.2	3.2
Averages:	25.5	14.6	9.6	5.3

*See Table 4 footnote.

Table 12
Ephemeris Differences Between Overlapping DE-2 Orbit Solutions
That Included Estimation of Random Drag Forces

Comparison Interval*	Maximum Overlap Differences (Meters)			
	One Impulse	Two Impulses	Three Impulses	Four Impulses
1A-1B	138	125	215	320
1B-1C	243	151	119	159
1C-1D	178	135	143	105
1D-1E	184	89	97	55
1E-1F	387	146	217	257
Averages:	226	129	158	179
4A-4B	2035	998	974	561
4B-4C	835	226	210	446
4C-4D	1123	764	807	711
4D-4E	624	838	437	506
4E-4F	1337	888	385	263
Averages:	1191	743	563	497

*See Table 5 footnote.

Table 13
Solved-for Values of Along-Track Impulses Placed at Selected Perigee Points in DE-2 Orbit Solutions

Solution Interval*	Solved-for Values of Impulses (Centimeters/Second)									
	One Impulse	Two Impulses		Three Impulses			Four Impulses			
	S1	S1	S2	S1	S2	S3	S1	S2	S3	S4
1A	−0.10	−0.07	0.33	−1.25	−0.63	−1.00	−0.70	0.70	−0.00	0.62
1B	−0.41	0.41	−0.01	−0.50	−0.70	−0.69	−0.78	2.00	0.58	−1.45
1C	0.48	0.27	−0.46	0.11	−0.12	−0.59	0.23	−0.00	−0.37	−0.58
1D	−0.30	−0.41	−0.36	−0.26	−0.50	−0.37	−0.56	−0.58	−0.60	−0.57
1E	1.49	0.92	−0.24	0.60	2.27	−1.03	−1.26	−0.19	−0.05	−2.13
1F	−0.91	−3.00	−1.79	−0.03	0.68	4.14	−0.72	−2.58	−1.70	−1.00
Averages:	0.62	0.69		0.86			0.83			
4A	1.00	5.50	−1.39	7.41	5.30	−0.38	−0.19	0.35	−1.92	−4.37
4B	−2.17	−4.38	−3.03	−2.24	−2.00	2.31	−0.22	0.35	1.71	3.93
4C	0.29	4.32	4.88	1.04	1.06	−2.31	1.93	5.07	1.86	0.05
4D	−1.78	−2.71	0.08	3.51	1.77	2.83	5.12	2.17	3.21	5.45
4E	.65	0.79	−0.67	−0.40	0.63	−0.08	−1.19	−0.08	−0.78	0.37
4F	−1.02	1.85	−0.33	1.94	−1.96	−1.58	1.69	−1.62	−2.25	0.00
Averages:	1.15	2.49		1.61			1.76			

*See Table 4 footnote.

Table 14
Correlation Coefficients from a DE-2 Orbit Solutions in
Which Three Perigee Impulses Were Estimated

Solution Interval*	Correlation Coefficient					
	(RHO1, S1)	(RHO1, S2)	(RHO1, S3)	(S1, S2)	(S1, S3)	(S2, S3)
4A	.965	.925	.911	.820	.900	.789
4B	.947	.869	.737	.692	.823	.344
4C	.958	.939	.806	.812	.843	.649
4D	.702	.965	.810	.524	.473	.761
4E	.769	.950	.897	.608	.878	.759
4F	.770	.947	.970	.695	.759	.864

*See Table 4 footnote.

Table 15
DE-2 Prediction Accuracy Using the Last Definitive Values of RHO1 (GEM9 21 X 21)

Epoch (1983)	Maximum Along-Track Error (Kilometers)							
	Prediction Interval (Days)							
	1	2	3	4	5	6	7	8
Jan 14, 0^h	3	30	X	X	175	186	156	X
Jan 14, 12^h	17	56	X	X	162	193	186	129
Jan 15, 0^h	-1	X	X	-93	-222	-435	X	X
Jan 15, 12^h	-10	X	X	-114	-249	-471	-795	X
Jan 16, 0^h	X	X	-15	-88	-227	X	X	X
Jan 16. 12^h	X	X	-65	-170	-356	-637	X	X

Note: The GEM9 21 X 21 and the F#225 Harris-Priester models were used. The last definitive value of RHO1 was used in each prediction.

Table 16
DE-2 Prediction Accuracy Using the Last Definitive Values of RHO1 (GEM9 8 × 8)

Epoch (1983)	Maximum Along-Track Error (Kilometers)							
	Prediction Interval (Days)							
	1	2	3	4	5	6	7	8
Jan 14, 0^h	3	28	X	X	159	163	123	X
Jan 14, 12^h	16	54	X	X	150	173	158	89
Jan 15, 0^h	3	X	X	−78	−200	−405	X	X
Jan 15, 12^h	−11	X	X	−123	−265	−496	−832	X
Jan 16, 0^h	X	X	−28	−110	−261	X	X	X
Jan 16, 12^h	X	X	−63	−164	−345	−621	X	X

Note: The GEM9 8 × 8 and the F#150 Harris-Priester models were used in each prediction. The last definitive value of RHO1 was used in each prediction.

Table 17
DE-2 Prediction Accuracy Using the Average Value of RHO1
for the Prediction Interval

Epoch (1983)	Maximum Along-Track Error (Kilometers)							
	Prediction Interval (Days)							
	1	2	3	4	5	6	7	8
Jan 14, 0^h	17	64	X	X	330	401	431	X
Jan 14, 12^h	32	93	X	X	278	365	42C	431
Jan 15, 0^h	56	X	X	327	404	441	X	X
Jan 15, 12^h	64	X	X	236	323	382	399	X
Jan 16, 0^h	X	X	202	265	298	X	X	X
Jan 16, 12^h	X	X	130	198	246	260	X	X

Note: The GEM9 21 X 21 and the F#225 Harris-Priester models were used. The value of RHO1 used in each prediction was the average of the definitive values of RHO1, obtained from the definitive solutions during the prediction interval.

Table 18
DE-2 Prediction Accuracy Using a Sectioned Linearly Varying Value of RHO1 in the Prediction Interval

Epoch (1983)	Maximum Along-Track Error (Kilometers)							
	Prediction Interval (Days)							
	1	2	3	4	5	6	7	8
Jan 14, 0^h	1.5	1.1	X	X	−5.3	6.2	4.8	X
Jan 14, 12^h	−2.3	−4.8	X	X	−5.4	−2.5	−4.1	−4.6
Jan 15, 0^h	3.9	X	X	19.1	23.4	26.1	X	X
Jan 15, 12^h	−1.7	X	X	3.1	7.0	8.2	10.4	X
Jan 16, 0^h	X	X	−5.9	−6.6	−9.1	X	X	X
Jan 16, 12^h	X	X	16.0	25.1	31.7	39.7	X	X

Note: The GEM9 8 X 8 and the F#150 Harris-Priester models were used in each prediction. A linearly-varying approximation for RHO1, based upon the definitive values of RHO1 during the prediction interval, was used in each prediction.